

# Structure, Microhardness and Magnetic Properties of Electroplated Ni-Cu Alloys

Mosaad Negem<sup>a</sup>, M.Y.F. Elzayat<sup>b\*</sup>

<sup>a</sup> Chemistry Department Faculty of Science Fayoum University, Egypt

<sup>b</sup> Physics Department Faculty of Science Fayoum University, Egypt

E-mail address: myfelzayat@yahoo.com

*Ni-Cu alloys were electroplated from sulphate bath using addition agents including sodium gluconate, boric acid and cysteine on a copper sheet by the galvanostatic method and ultrasound waves. The surface morphology, chemical composition, crystalline structure, magnetic properties and hardness of the Ni-Cu alloys were investigated using scanning electron microscope, energy dispersive spectroscopy, X-ray diffraction, vibrating sample magnetometer and Vickers testing method. The use of the appropriate concentrations of the addition agent simultaneously with the conventional ultrasound waves (CUW) during sample preparation was found to produce nanocrystalline Ni-Cu alloys. XRD patterns showed the existence of two planes of 111 and 200 for the Ni-Cu alloys. The microhardness of the Ni-Cu alloys varied between 150 HV and 440 HV. The mechanical properties of nanocrystalline Ni-Cu alloys showed an increase of the hardness with increasing Ni content. The surface morphology of the coatings seemed to be the cauliflower and spherical grains. The increase of Ni content in the Ni-Cu alloys led to the formation of soft magnetic materials.*

## 1. Introduction

Ni-Cu alloys are widely used in many industries including craft, power stations, magnetoresistive sensors, decorative and protective fields, microelectromechanical systems (MEMS), and data storage devices in addition to their useful properties such as good corrosion resistance, distinct mechanical and thermo-physical properties, catalytic and magnetic properties [1-4]. The soft magnetic metals such as nickel in the nano-range are extremely important and can be applied for nanobiosensors, magnetic recording media and microelectromechanical systems [5,6]. However, few authors have studied the structural, magnetic, and microhardness properties of Ni-Cu coatings.

Metal nanoparticles show the exceptional electronic, catalytic and optical properties because of their size and distribution [7]. The most important factor

in the electroplating of the metals and alloys is the local mass transport near the cathode [8]. At the cathode, the decrease of metal ions causes undesirable side reaction because the metal ions have insufficient mass transport. Ultrasound waves produce high mass transport of reactive species and mechanically affect the electrochemical reactions happening onto the cathode. This leads to increase the cathodic current efficiency and decrease the required amount of the addition agents such as brightener during electroplating processes.

The mechanical properties of the Ni-Cu alloys depend on their grain size. The decrease of the grain size of alloys from the range of 1–100  $\mu\text{m}$  to the range of 10–100 nm leads to the significant enhancements in the strength and ductility that suggested by theoretical analyses [9]. Nonetheless, the production of nanocrystalline film is one of the considerable challenges since most techniques give imperfect materials attaining high levels of porosity or impurities [10]. However, the electroplating technique creates the homogenous coatings and is considered as a cheap technique.

Complexing agents, brighteners and antipitter (boric acid) improve the surface morphology of the electroplated metal and alloys. Electroplating of Ni-Cu alloys was performed in the presence of organic refiner such as saccharin. The hardest Ni coatings have high tensile intrinsic stress [11]. Addition of micromoles per litre of aliphatic organic sulphur-compounds, existing in the electrolyte, reduces the stress. The sulphur-compounds create bright and fine granular coatings. The present work pays attention to electroplating the nanocrystalline Ni-Cu alloys using addition agent and conventional ultrasound waves (CUW), and investigate the magnetic and microhardness properties of the Ni-Cu alloys.

## 2. Experimental Methods

TTiThurlby Thander instrument PL310 32V-1A PSU was used as the source of the direct current. Copper sheet (0.1mm thick) with purity of 99.98 % was the cathode, and a platinum mesh of 2.4  $\text{cm}^2$  acted as anode. The electroplating of the Ni-Cu alloys was carried out in Pyrex cylinder cell with Polytetrafluoroethylene (PTFE) lid which contains five holes. The hole cell is immersed in ultrasound bath and ice blocks were used to maintain room temperature. A 100 W ultrasonic bath of Branson 3510 with 42 KHz frequency was utilized as a source of ultrasonic waves. The electrolyte pH was obtained using the SevenMulti pH-metre and conductivity-metre from Mettler Toledo. The microhardness measurements were preceded in three positions on the sample of Ni-Cu alloys using a HMV-2000 Shimadzu microhardness tester (Vickers' microhardness instrument) with different loads of 50, 100 and 1000 g for 20 s. The magnetic hysteresis measurements were made using a Vibrating Sample Magnetometer (VSM, Model LDJ 9600-1,

USA) by cutting the alloys in the rectangle shape and varying the magnetic field intensity between  $\pm 20$  kOe parallel to the coating planes. The surface morphology of the coatings was examined using scanning electron microscopy (JOEL JSM-5300 LV, at 25 KV under high vacuum). Besides, the chemical composition of the coating was determined by energy dispersive X-ray analysis (EDX), which was incorporated with scanning electron microscopy. The crystalline structures of the coatings were determined by X-Ray diffraction with Philips X'Pert Pro Diffractometer, fitted with the X'Celerator and a secondary monochromator. To generate copper K- $\alpha$  radiation with wavelength of  $1.54 \text{ \AA}$ , a copper anode was supplied with the current of 0.04 A and the voltage of 40000 V. Electroplating electrolytes were prepared using the chemicals of Aldrich, Sigma and Merck grade. The chemicals were  $\text{NiSO}_4 \cdot 7\text{H}_2\text{O}$ ,  $\text{CuSO}_4 \cdot 5\text{H}_2\text{O}$ ,  $\text{H}_3\text{BO}_3$ , sodium gluconate and cysteine. The chemicals were weighed and dissolved in deionized water to obtain the molar ratio, as shown in Table (1).

**Table (1):** composition of electrodeposition baths was utilized to electrodeposit Ni and Ni-Cu alloys using conventional ultrasound waves at 293 K for 1 hour.

Bath	$\text{NiSO}_4$ M	Composition $\text{CuSO}_4$ M	Sodium gluconate M	$\text{H}_3\text{BO}_3$ g/l	Cysteine mM	Operating pH	Conditions Current density $\text{A/cm}^2$	Conductivity $\text{mS/cm}^2$
1	0.1000	-	0.1	10	0.18	4.1	0.025	11.40
2	0.0995	0.0005	0.1	10	0.18	4.0	0.025	11.31
3	0.0980	0.0020	0.1	10	0.18	4.1	0.025	11.40
4	0.0950	0.0050	0.1	10	0.18	4.1	0.025	11.80
5	0.0935	0.0065	0.1	10	0.18	4.1	0.025	11.10
6	0.0925	0.0075	0.1	10	0.18	4.1	0.025	11.17
7	0.0900	0.0100	0.1	10	0.18	4.0	0.025	11.50
8	0.0500	0.0500	0.1	10	0.18	3.8	0.025	11.75
9	-	0.1000	0.1	10	0.18	3.5	0.025	11.10

The electroplating of Ni, Cu and their alloys was performed from ultrasonicated electrolytes using current density of  $0.025 \text{ A/cm}^2$  which is the experimental optimized value. Also, different concentrations of sodium gluconate, cysteine and boric acid were utilized to optimize the bath. The optimized concentrations of these chemicals were recorded in table 1. The electroplating time was one hour at 293 K. Freshly prepared electrolyte was prepared for each experiment to overcome the change in the electrolyte properties and the concentration of the components. Prior to each run, the copper sheet was etched using concentrated nitric acid (1:1) for just one minute to remove the oxide layers, and then washed with deionized water, then rinsed with acetone.

### 3. Results and Discussion

#### 3.1. SEM and Composition of the Ni-Cu Alloys

Figure (1) shows scanning electron microscopy (SEM) images of nanocrystalline Ni-Cu alloys obtained using gluconate bath and CUW at a current density of  $0.025\text{A/m}^2$ . The CUW and addition agents significantly improve the surface morphology, nanostructure and the properties of the electroplated Ni-Cu alloys. The addition agents involved sodium gluconate, and cysteine as well as boric acid. The effect of the CUW is due to the removal of hydrogen bubbles from the cathode surface producing fine coatings [12]. It was revealed that acoustic streaming, microjets and shock waves improve greatly the thin film obtained from the electroplating [13].

Sodium gluconate added to electrolyte acts as ligand for Ni and Cu ions, produces the fine grains, and create the regular and granular nickel. This may result from the formation of Ni-gluconate complex which accelerates the transfer of electrons via ion bridging [14] and shifts the reduction potential to more positive direction. Moreover, the morphology of Ni and Ni-Cu alloys are various as a result of the different nucleation growth rates and addition agents. In acidic aqueous medium ( $\text{pH} < 7$ ),  $\text{Ni}^{2+}$  reacted with sodium gluconate to form complexes as shown in previous work [12]. The gluconate ion is attached to Ni and Cu ions by coordination through the carboxyl group and one of the adjacent hydroxyl groups [15].

Boric acid has a great effect on the morphology of the Ni-Cu alloys; it produced the fine, dense and granular Ni-Cu alloys. Therefore, it has significant role more than a buffer. Using cathodic polarization, the effect of boric acid is proved to move the reduction potential of Ni to more positive direction than hydrogen and shifts the reduction potential of Ni near the reduction potential of Cu [12]. Also, the  $\text{Ni}^{2+}$  and  $\text{Cu}^{2+}$ -boric acid complexes act as fine catalyst and adhere on the cathode surface [16]. It was suggested that boric acid is adsorbed on the cathode surface, and thus lowers the active area for hydrogen evolution by different ions formed as clear in the previous study [15]. Thus affects the resulting morphology characteristics of the thin film [17] producing a fine and granular coating as in Fig (1). Also, boric acid stabilizes evidently the surface pH. Adsorption of boric acid on the cathode decreases the effective surface available for proton reduction [18]. Moreover, many researchers confirmed that the boric acid behaves like the surfactant, which adsorbs on the surface. The authors attributed the observed changes in surface morphology to a weak boric acid adsorption mechanism.

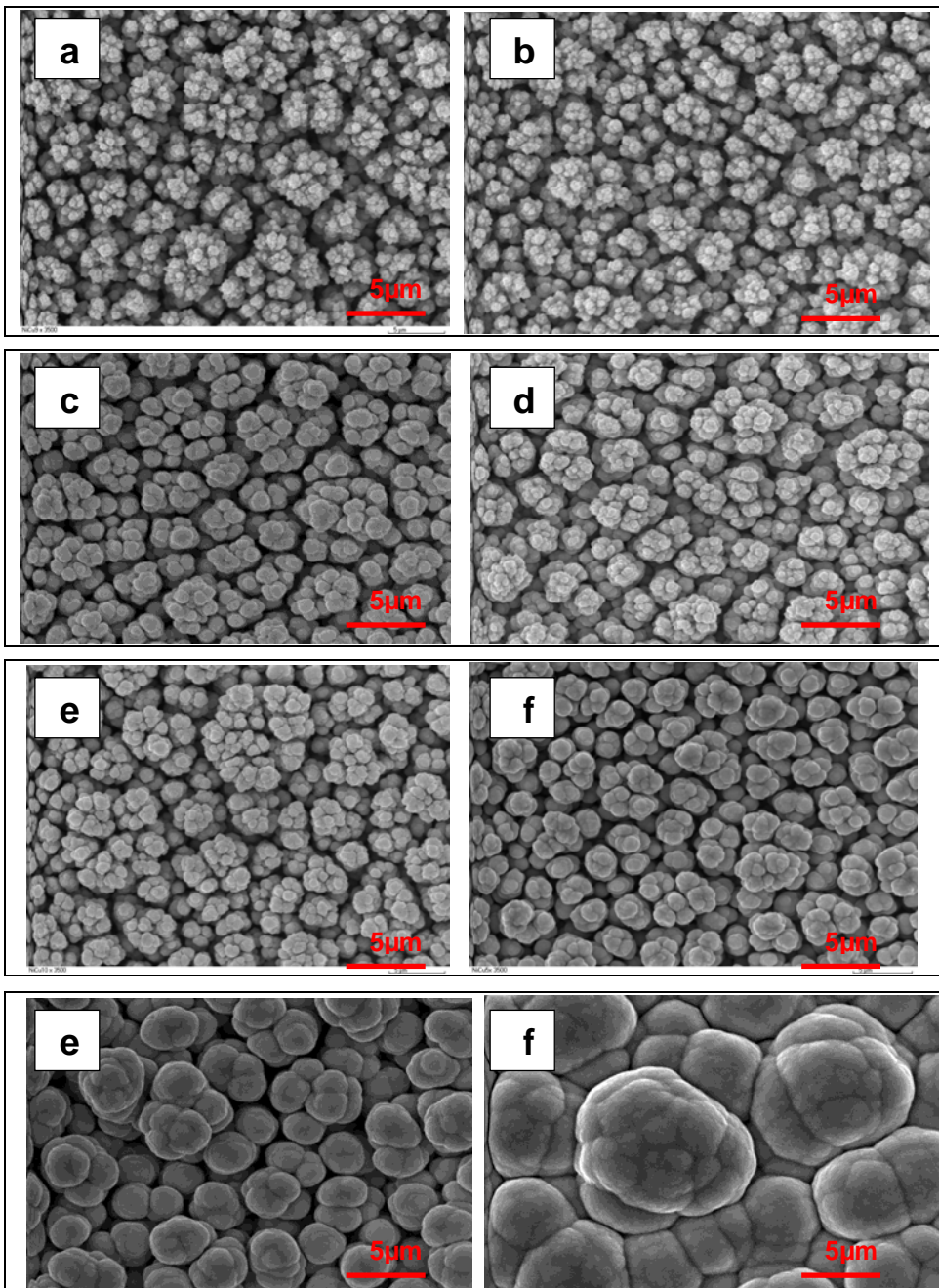


**Fig. (1):** Morphological structure (SEM) of nanocrystalline Ni, Cu and Ni-Cu alloys produced using the conventional ultrasound waves for 1 hour at 293 K, where: a. Ni-19Cu; b. Ni-26Cu; c. Ni-44.5Cu, d. Ni-49Cu, e. Ni-59Cu; f. Ni-86Cu; g. Ni-94Cu and h. pure Cu.

To optimize the electroplating process, different current densities between 0.005 and 0.12 A/cm<sup>2</sup> were used. It was found that the surface morphology of Ni coating was slightly affected by the increase of the current densities between 0.005 -0.12 A/cm<sup>2</sup> in the presence of CUW. The CUW eliminated pores from the coated Ni as compared to that obtained from silent solution. However, the increase of current density more than 0.025 A/cm<sup>2</sup> produced very rough thin film of Ni-Cu alloys.

Cysteine made a dense, smooth and shiny Ni (but not shown). The size of the grains was increased with the increase of Cu content from 49% to 99% for the Ni-Cu alloys.

The cysteine adsorbs at the electrode surface and forms a complex with Ni and Cu ions which ascribes to the interaction of ion pair of electrons of N, S and O atoms (produced from addition agents). It was observed that the carboxyl group of cysteine has no reaction with the metal ions and that the maximum number of the cysteine molecules bound to the Ni (II) ion is two. Hence Ni (II) in bis-cysteino-Ni (II) is tetracoordinated.

Cysteine adsorbs at the cathode substrate and produces layer with powerful interaction [19]. It also behaves as a non-blocking adsorber which happens on the active sites of the crystal planes of the cathode and on the emerging surfaces of the crystallizing phases [19]. Consequently, it can act as an obstacle to decelerate surface diffusion of adsorbed ions [20]. This causes a more difficult grain growth and hence forming fine grains and the structures become more compact which is similar to saccharin [21]. The different Ni-Cu alloys are obtained using gluconate bath, however the growth of Cu<sup>2+</sup> concentration increases sharply in the alloys due to the more positive of the reduction potential of Cu than Ni.

The increase of Cu content in the Ni-Cu alloys changes the morphology from cauliflower to granular structure as a result of the decrease of grain size Fig.(1). However, the gluconate-cysteine bath and CUW produce smooth and dense pure Ni and pure Cu. Consequently, it turned out that the alteration in surface morphology is related to the change of crystal structure caused by addition agent and CUW. This is because of the different electroplating parameters that have considerable effect on morphological structure of the alloys such as electrolyte pH, temperature, or addition agent in bath as well as the use of CUW. Researchers [22] optimized deposition parameters and generated uniform and fine grained surfaces from acid chloride-sulphate bath while the present study produces fine surfaces from sulphate bath alone. Although study [23] emphasized that low stressed thin film was obtained from sulphamate electrolyte, different deposit quality reported in the present work

may be due to different substrate, sulphate-cysteine bath or ultrasound waves used through the electroplating.

Energy dispersive X-ray analysis showed that the nanocrystalline Ni obtained from baths 1 was about 99.99%. In addition, the different Ni-Cu alloys were electroplated from gluconate bath with the various Cu content, as can be seen in Table (2). The variation of Cu content of the Ni-Cu alloys was between 19 % and 99.9 % which was developed by the change of  $\text{Ni}^{2+}$  and  $\text{Cu}^{2+}$  concentrations in the electrolytes. Also, the pure Cu was obtained as can be seen in Table (2).

**Table (2):** Chemical compositions of nanocoated Ni and Ni-Cu alloys obtained using conventional ultrasound waves and additives at 293 K for 1 hour from EDX analysis.

coating	Ni%	Cu%
1	99.9	-
2	81	19
3	74	26
4	56	44
5	51	49
6	41	59
7	14	86
8	6	94
9	-	99.9

### 3.2. Structural examination of Ni-Cu alloys

Figure (2) shows the XRD patterns of the pure Ni, pure Cu and Ni-Cu alloys electroplated as mentioned above. The nanocrystalline Ni-Cu alloys displayed the FCC structures of two characteristic crystal planes, (111) and (200). The plane (111) showed two peaks which appeared obviously at  $2\theta$  of  $43^\circ$  and  $44.4^\circ$ , respectively. In addition, the intensity of (200) plane decreased with increasing % Cu for the Ni-Cu alloys from  $2\theta$  of  $50^\circ$  and  $51.9^\circ$ . However, the pure Ni, pure Cu and Ni-94Cu alloy displayed one peak for each plane.

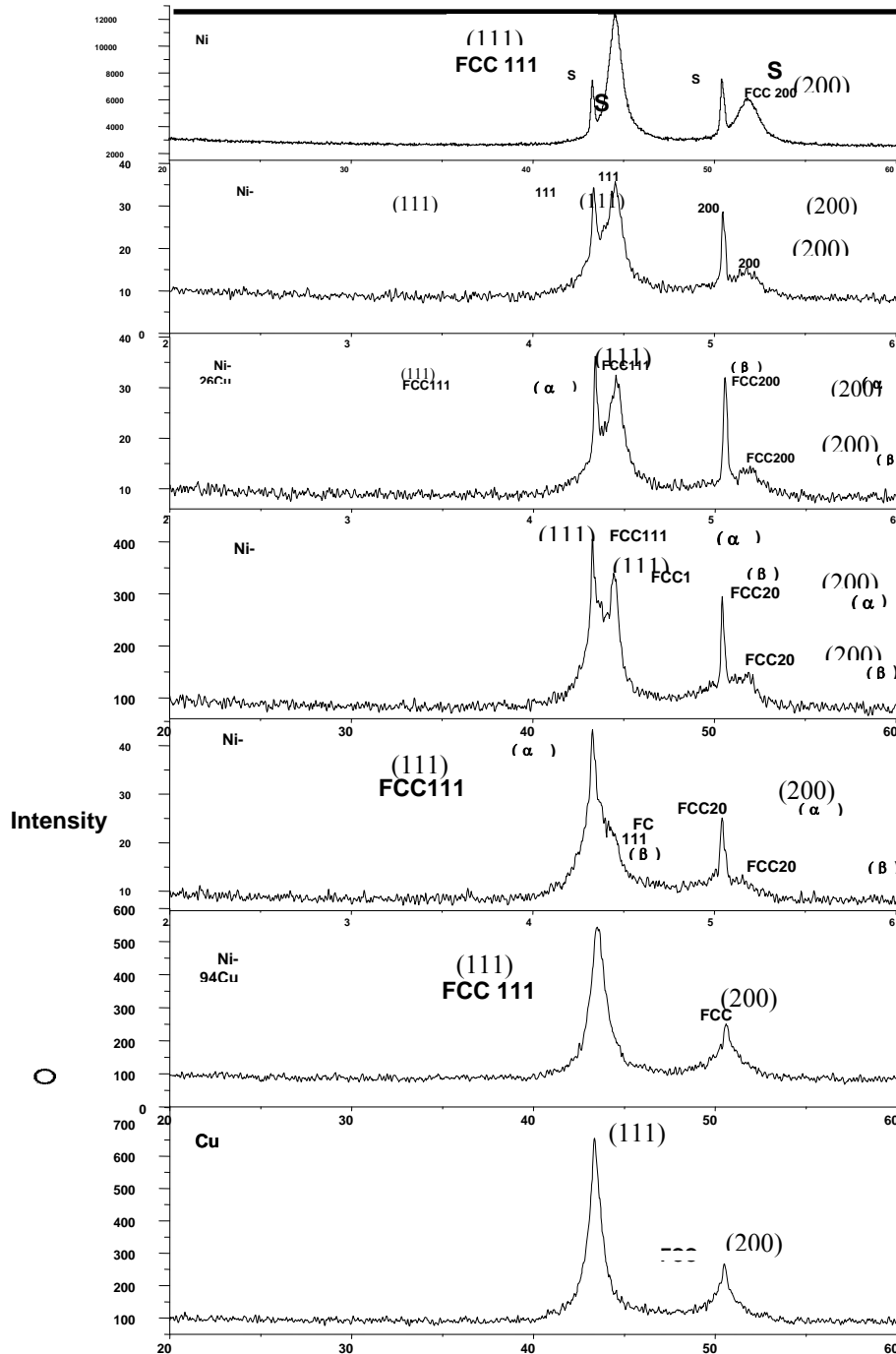
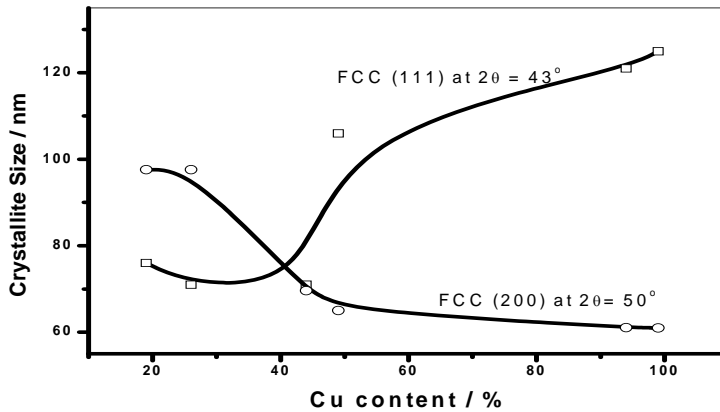


Fig. (2): XRD patterns of nanocrystalline Ni-Cu alloys obtained from gluconate bath using conventional ultrasound waves and a current density of 0.025 A/cm<sup>2</sup> for 1 hour.

The average crystalline size of the pure Ni, pure Cu and Ni-Cu alloys was calculated using Debye-Scherer's equation [24]:  $\tau = K\lambda / \beta \cos \theta$  where  $\lambda$  is the x-ray wavelength, typically 1.54 Å,  $\beta$  is the line broadening at half maximum intensity in radians, K is the shape factor, and  $\theta$  is the Bragg angle;  $\tau$  is the mean size of the ordered (crystalline) size.

Figure (3a) shows that the crystallite size of nanocrystalline Ni-Cu alloys calculated for the (111) peak at  $2\theta = 43^\circ$  varied between approximately 72- 130 nm with the % Cu range from 19 up to 99.9%. The crystallite size of (200) peak at  $2\theta = 50^\circ$  for Ni-Cu alloys declined gradually from 90nm to 62nm with the increase of %Cu.



**Fig. (3a):** Variation of particle size of FCC structure of Ni-Cu alloys with Cu content.

In addition, the crystallite size calculated from the (111) peak at  $2\theta = 44^\circ$  decreased sharply from 47 nm to 13 nm for Ni content range from 74 to 99.99%. The other (200) peak at  $2\theta = 51.9^\circ$  gave a gradual decrease of crystallite size from 26 nm to 16 nm then increased to 21 nm as shown in Fig. (3b).

In fact, the crystallite size of Ni, Cu and their alloys was greatly changed to homogenous rather than inhomogeneous as a result of using the CUW and the addition agent [12]. This may be due to the nucleation rate and the arrangement of the additive molecules on the cathode surface, and instantaneous removal of  $H_2$ . It can also be caused by the high mobility of ions decreasing the resistance polarization, high temperature and surface cleaning caused by shear stress. The formation of two peaks of each plane may be as a result of the presence of hot spot created by ultrasound waves. The effect of increase temperature on the formation of peaks for the Ni-Cu alloys was also reported in [5]. This effect is due to the shift of the cathodic potential towards more positive values with a rise of the temperature of the bath at hot spot places obtained from ultrasound waves, leading to the production of the different peaks.

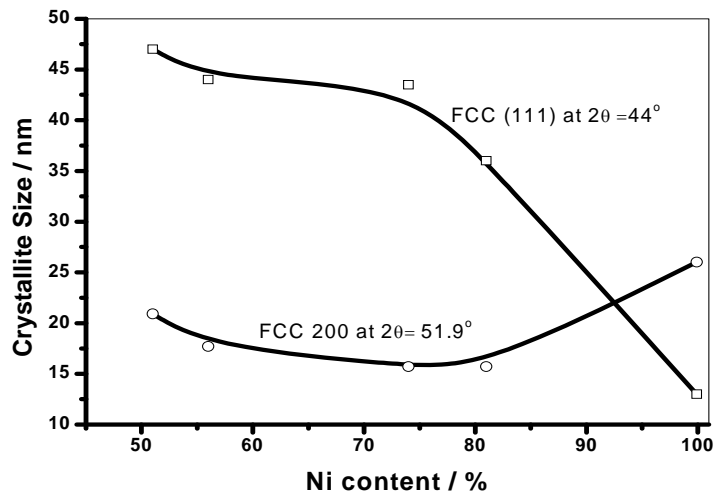


Fig. (3b): Variation of particle size of FCC structure of Ni-Cu alloys with Ni content.

### 3.3. Microhardness of Ni-Cu Alloys

Figure (4) shows the variation of microhardness of Ni-Cu alloys samples. The microhardness of Ni-Cu alloys was greatly affected by the Ni content and particle size. The microhardness of Ni-Cu alloys increased first gradually with the Ni content then it increased sharply. Moreover, it can be seen that the pure Ni possessed the highest microhardness of 440 HV while the pure Cu displayed the lowest value of the microhardness of 150 HV. These values of hardness of Ni-Cu alloys are higher than those obtained with silently electroplated Ni [12]. This may be due to using the CUW and addition agent in the preparation technique. This observation of refinement effect is consistent with [20] who concluded that the incorporation of organic addition agent (cysteine) into the plating bath resulted in inhibition of granular growth, reduction of surface roughness, increase in surface brightness and sharp reduction of grain size. The smoothness of the surface has been shown by Beacon et.al [25] to be dependent on the distribution of addition agents.

The increase in the hardness of the Ni-Cu alloys with the increase of Ni content result from the increase of planes crystal structure of Ni-rich alloys possessing smaller grain size than that of Cu-rich alloys. It was reported that smaller grains displayed higher hardness [23]. Indeed, similar results were revealed that the nanocrystalline Ni-Cu coatings exhibit a higher hardness with the increase of the Ni content in the alloys [26]. Actually, strengthening the poly-nanocrystalline materials is technologically attractive due to the stabilization in their toughness and ductility. Ultrasonic waves produce hard coatings because of formation of smaller grain size [27]. Also, the microhardness of Ni-Cu alloys can be increased due to use of addition agent

such as cysteine as brightener due to formation of fine nanocrystalline grains. The nanocrystalline coatings improved the mechanical properties, higher hardness and elastic recovery and good wear resistance [26]. Moreover, the hardening effect by addition agent is understandable when grain refinement effect is taken into account [28]. In fact, it has long been known that the mechanical properties of polycrystalline metals and alloys depend on their grain size. In many cases, the hardness varies with the grain size according to the Hall–Petch relationship [29]. It is clear that the strength and hardness of a metallic material significantly increase when the grain size decreases.

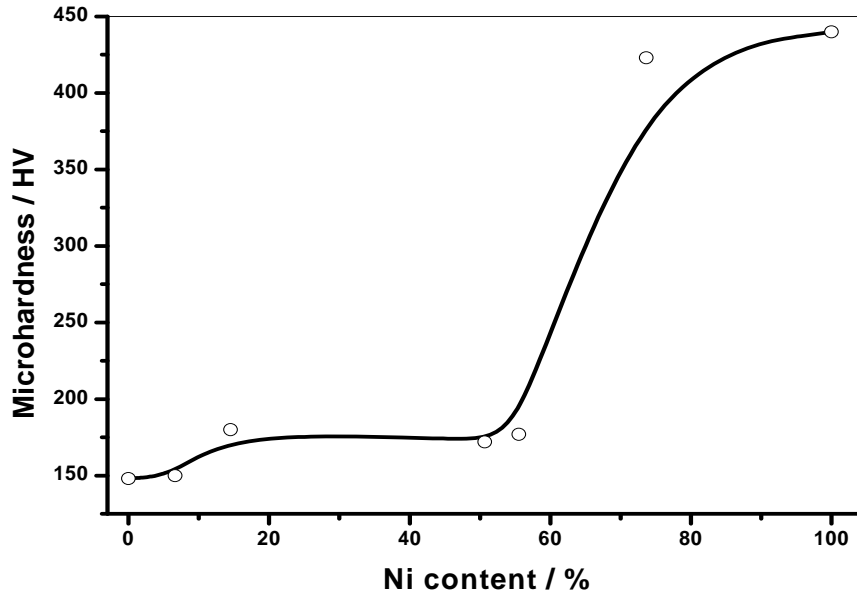


**Fig. (4):** Variation of microhardness of Ni-Cu alloys with Ni content obtained from gluconate bath using conventional ultrasound waves and current density of  $0.025 \text{ A/cm}^2$  for 1 hour at 293 K.

### 3.4. Magnetization of the Ni-Cu alloys

Figure (5a) shows the hysteresis loops obtained for pure Ni, pure Cu and their alloys with different Ni content. The hysteresis parameters, namely saturation magnetisation ( $M_s$ ) and parallel coercivity ( $H_c$ ) for all the deposits, are shown in Fig. (5b and 5c). As the Ni content increased the  $M_s$  increased also such that the pure Ni displayed the highest magnetisation value of  $458 \text{ emu/cm}^3$  while the Ni-94Cu alloys showed the lowest magnetisation of  $10 \text{ emu/cm}^3$ , as can be seen in Fig. (5b). The  $H_c$  values decreased gradually then sharply with the increase of Ni content. The lowest value of  $H_c$  was about 87.5 Oe for the pure Ni but the highest  $H_c$  value was about 252 Oe for Ni-94Cu as can be seen in Fig (5c).

The Ni-Cu alloys displayed the high  $M_s$  values with the increase Ni content, which is confirmed by the study in [30]. The general increasing trend in  $M_s$  with increasing Ni can be understood as a consequence of the dominance of the ferromagnetic character of nickel, since Ni has higher magnetic dipole moment while Cu is diamagnetic materials, it is expected that the Ni-Cu alloy highly rich with Cu would be diamagnetic[30]. Consequently, the  $M_s$  of the Ni-Cu alloys depends completely on Ni content. Moreover, the decrease of  $M_s$  was due to an increase of Cu content of the Ni-Cu alloys, which is similar to the result obtained by [31]. The coercivity shows wide fluctuations in the given compositional range, with high values for certain deposits. The pinning of domain wall energy by a second phase in the ferromagnetic matrix, dislocations and/or internal stress fields, as well as anisotropy due to surface and particle shape, are important factors that can increase the coercivity [32]. Comparing the different Ni-Cu alloys, the small grains of pure Ni and Ni-rich alloys show the more soft magnetic alloys than the Ni-Cu alloys of larger grain size of Cu-rich alloys. In fact, the current study and [33] indicate that  $H_c$  depends greatly on Ni content for the alloys created from sulphate bath. The change of  $H_c$  can be attributed to the variations in grain structures of the Ni-Cu alloys. It was emphasized that favoured grain structures have an effect on the  $H_c$  of the coatings [34], the small grain sizes lower the  $H_c$ . Also, the various electroplating conditions can affect the  $H_c$  [34]. Nonetheless, it was postulated that the spherical grains causes a formation of hard magnetic coatings [35], seeing that the growth of Cu content in the Ni-Cu alloys enhances the spherical morphologies, while the pure Ni and Ni-rich alloys show soft magnetic performance. Comparing the different Ni-Cu alloys, the small grains of the pure Ni and Ni-rich alloys show the more soft magnetic alloys than the Ni-Cu alloys of larger grain size of Cu-rich alloys.

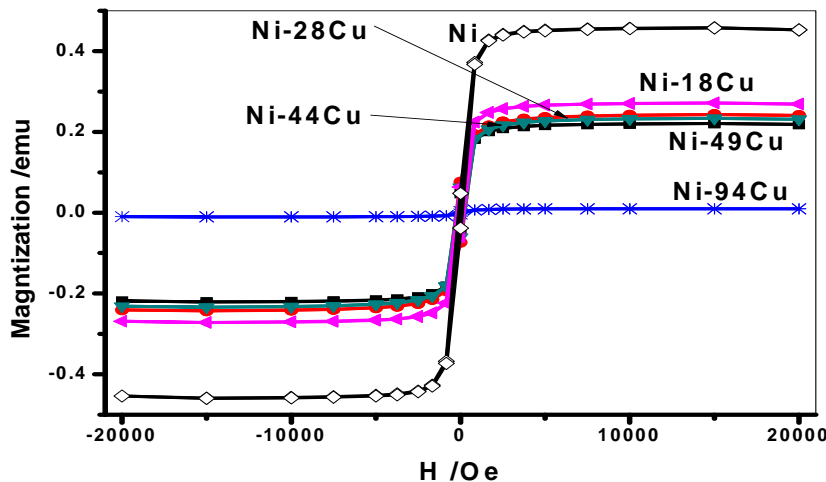


Fig. (5a): the parallel plane hysteresis loops of Ni-Cu alloys obtained using the conventional ultrasound waves and a current density of  $0.025 \text{ A/cm}^2$

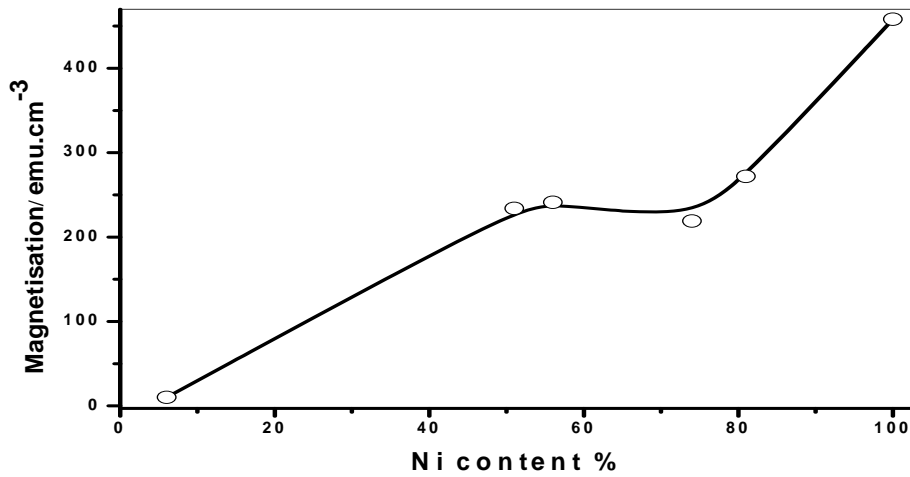


Fig. (5b): Variation of magnetization with Ni content of Ni–Cu alloys obtained using the conventional ultrasound waves and a current density of  $0.025 \text{ A/cm}^2$

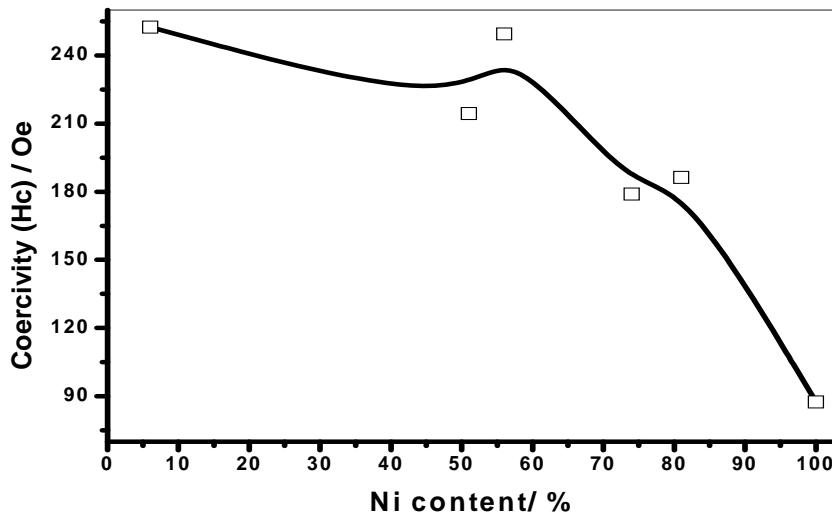


Fig. (5c): Variation of coercivity with Ni content of Ni–Cu alloys obtained using the conventional ultrasound waves and a current density of  $0.025 \text{ A/cm}^2$

#### 4. Conclusion

The surface morphology of Ni and Ni-Cu alloys was improved as a result of adding sodium gluconate, boric acid, cysteine and the use of the conventional ultrasound waves. The addition agent and conventional ultrasound waves produced nanocrystalline Ni and Ni-Cu alloys. Different current densities of  $0.005$  to  $0.12 \text{ A/cm}^2$  were operated to optimize the electroplating of Ni-Cu alloys. The conventional ultrasound waves developed the electroplating at high

current density of  $.0025 \text{ A/cm}^2$ . The microhardness of the Ni-Cu alloys was significantly affected due to the change of Ni content, and its value varied between 150 and 440 HV. The pure Ni displayed the highest magnetisation of  $458 \text{ emu/cm}^3$  and lowest coercivity of 87.5 Oe. The increase of Ni content in the Ni-Cu led to the formation of the soft magnetic materials.

## 5. References

1. S. Wang, X. Guo, H. Yang, J. Dai, R. Zhu, J. Gong, L. Peng, and W. Ding, *Appl. Surf. Sci.*, **288**, 530 (2014).
2. N. Myung, and K. Nobe, *J. Electrochem. Soc.*, **148**, C136.(2001)
3. A. Foyet, A. Hauser, and W. Schäfer, *J. Solid State Electrochem.* 12.47 (2008).
4. S. Ghosh, G. Dey, R. Dusane, and A. Grover, *J. Alloys Compd.*, 426. 235 (2006).
5. U. Sarac, and M. Baykul, *J. Allo. Compds.*, **552**. 195 (2013)
6. J. Qin, J. Nogues, M. Mikhaylova, A. Roig, J. Munoz, and M. Muhammed, *Chem. Mater.*, **17**, 1829 (2005).
7. M. Watanabe, T. Akimoto, and E. Kondoh, *ECS J. Solid State Sci. Tech.*, **2**, M9 (2013).
8. J. Jensen, P. Pociwardowski, P. Persson, L. Hultman, and P. Moller, *Chem. Phys. Lett.*, **368**. 732 (2003).
9. A. Giga, Y. Kimoto, and Y. Takigawa, *Scripta Mater.*, **55**. 143. (2006)
10. Y. Li, H. Jiang, and L. Pang, *Surf. Coat. Tech.*, **201**.5925 (2007).
11. A. Bhandari, S. Hearne, B. Sheldon, and S. Soni, *J. Electrochem. Soc.*, **156**. D279 (2009).
12. H. El-feky, M. Negem, S. Roy, N. Helal, and A. Baraka, *Sci. China Chem.*, **1446**, 56 (2013).
13. R. Walker, and C. Walker, *Ultrasonics*, **13**. 79 (1975).
14. T. Franklin, *Surf. Coat. Tech.*, **30**. 415 (1987).
15. S. Abd El Rehim, M. Ibrahim, and M. Dankeria, *J. of Appl. Electrochem.* **32**, 1019 (2002).
16. S. Abd El Rehim, S. Abd El Wahaab, S. Rashwan, Anwar, *Z. J. Chem Technol Biotechnol*, **75**. 237 (2000).
17. J. Horkans, *J. Electrochem Soc*, **126**. 1861 (1979).
18. N. Zech and D. Landolt, *Electrochim. Acta*, **45**, 3461 (2000).
19. T. Osaka, T. Sawaguchi, F. Mizutani, T. Yokoshima, M. Takai, and Y. Okinaka, *J. Electrochem. Soc.*, **146**, 3295 (1999).
20. Y. Li, H. Jiang, D. Wang, and H. Ge, *Surf. Coat. Tech.*, **202**. 4952 (2008).
21. Ciszewski, S. Posluszny, G. Milczarek, and M. Baraniak, *Surf. Coat. Tech.*, **183**, 127 (2004).
22. Y. Yang, B. Deng, and Z. Wen, *Adv. Chem. Eng. Sci.*, **1**, 27 (2011).

23. M. Srivastava, V. Selvi, V. Grips, and K. Rajam, *Surf. Coat. Tech.*, **201**, 3051 (2006).
24. H. Klung, L. Alexander, John Wiley, New York, p. 618. (1974).
25. S. Beacon and B. Riley, *General Motors Engrg. J.*, 6.21(1959).
26. E. Pellicer, A. Varea, S. Pané, K. Sivaraman, B. Nelson, S. Suriñach, M. Baró, and J. Sort, *Surf. Coat. Tech.*, **205**, 5285 (2011).
27. S. Kochergin, and G. Vyaselva, *Electrodeposition of Metals in Ultrasonic Fields*. Ed. Consultants Bureau, New York, p. 19. (1966).
28. J. Vijayakumar, S. Mohan, and S. Yadav, *J. Alloys and Comp.* **509**, 9692 (2011).
29. A. Zimmerman, G. Palumbo, K. Aust, and U. Erb, *Mater. Sci. Eng. A* **328**, 137 (2002).
30. U. Sarac, and M. Baykul, *J. Supercond. Nov. Magn.*, **26**, 1753 (2013).
31. E. Gomez, S. Pane, and E. Valles, *Electrochim. Acta*, **51**, 146 (2005).
32. D. Jiles, in *'Introduction to Magnetism and Magnetic Materials'*, Chapman Hall, London, p.146. (1991).
33. D. Kim, D. Park, B. Yoo, P. Sumodjo, and N. Myung, *Electroch. Acta*, **48**, 819 (2003).
34. I. Rahman, M. Khaddem-Mousavi, A. Gandhi, T. Lynch, and M.A. Rahman, *J. Physics: Conference Series*, **61**, 523 (2007).
35. 35. A. Karpuz, H. Kockar, M. Alper, O. Karaagac, M. Hacıismailoglu, *App. Surf. Sci.*, **258**, 4005 (2012).